J|A|C|S
ARTICLES

Published on Web 01/20/2009

Size-Dependent Kinetic Enhancement in Hydrogen Absorption and Desorption of the Li−Mg−N−H System

Yongfeng Liu, Kai Zhong, Kun Luo, Mingxia Gao, Hongge Pan,* and Qidong Wang

Department of Materials Science and Engineering, Zhejiang University, Hangzhou 310027, People's Republic of China

Received August 19, 2008; E-mail: hgpan@zju.edu.cn

Abstract: High operating temperature and slow kinetics retard the practical applications of the Li−Mg−N−H system for hydrogen storage. To alleviate these problems, a first attempt was carried out by synthesizing $Li_2MgN_2H_2$ through sintering a mixture of $Mg(NH_2)_2$−$2LiNH_2$ and investigating its size-dependent hydrogen storage performance. A dramatically enhanced kinetics for hydrogen absorption/desorption was achieved with a reduction in the particle size. For the dehydrogenation reaction, a three-dimensional diffusion-controlled kinetic mechanism was identified for the first time by analyzing isothermal hydrogen desorption curves with a linear plot method. The experimental improvement and mechanistic understanding on the dehydrogenation kinetics of the Li−Mg−N−H system shed light on how to further decrease the operating temperature and enhance the hydrogen absorption/desorption rate of the amide/hydride combined materials.

1. Introduction

Hydrogen is the most ideal fuel in the comprehensive clean-energy concept. However, hydrogen storage is still a major technical barrier for its on-board application as a transportation fuel.[1,2] Presently many potential solid-state hydrogen storage materials in the metal−N−H systems, such as Li−N−H,[3−6] Li−Mg−N−H,[7−12] Li−Al−N−H,[13−16] Li−B−N−H,[17−19] Li−Mg−Al−N−H,[20,21] and so on, have been attracting significant attention owing to their high gravimetric hydrogen density. Among them, Li−Mg−N−H is regarded as one of the very promising systems because of its good reversibility, comparatively high hydrogen content, and favorable thermodynamic properties.[7−12] The $Mg(NH_2)_2$ and LiH mixture in the molar ratio of 1:2, which absorbs/desorbs 5.5 wt% of hydrogen according to the following reaction, attracted our attention:[7,8]

$$Mg(NH_2)_2 + 2LiH \leftrightarrow Li_2MgN_2H_2 + 2H_2 \quad (1)$$

According to the thermodynamic prediction, hydrogen desorption of eq 1 should occur at temperatures around 90 °C at 1.0 atm hydrogen pressure with a desorption enthalpy of 39 kJ/mol-H_2.[8,9] Unfortunately, a detectable rate of hydrogen desorption was experimentally attained only at temperatures above 200 °C, indicating the presence of a relatively high kinetic barrier for this reaction to be surmounted.[9]

For lowering the operating temperature and improving the hydrogen desorption kinetics of the metal−N−H systems, the reaction mechanism between amide and hydride needs to be understood. Up to now, several competing mechanism models have been proposed.[22−24] Chen et al. proposed the coordinated two-molecule or multimolecule reaction mechanism, believing that the dehydrogenation process proceeds via a direct solid−solid reaction which is driven by the strong affinity between the

(1) Schlapbach, L.; Züttel, A. *Nature* **2001**, *414*, 353–358.
(2) Multi-Year Research, Development and Demonstration Plan: Planned Program Activities for 2005−2015: Technical Plan; US Department of Energy; http://www.eere.energy.gov/hydrogenandfuelcells/mypp/pdfs/storage.pdf (Web release date October 23, 2007).
(3) Chen, P.; Xiong, Z. T.; Luo, J. Z.; Lin, J. Y.; Tan, K. L. *Nature* **2002**, *420*, 302–304.
(4) Ichikawa, T.; Hanada, N.; Isobe, S.; Leng, H. Y.; Fujii, H. *J. Alloys Compd.* **2005**, *404−406*, 435–438.
(5) Aguey-Zinsou, K. F.; Yao, J. H.; Guo, Z. X. *J. Phys. Chem. B* **2007**, *111*, 12531–12536.
(6) Xie, L.; Zheng, J.; Liu, Y.; Li, X. G. *Chem. Mater.* **2008**, *20*, 282–286.
(7) Xiong, Z. T.; Wu, G. T.; Hu, J. J.; Chen, P. *Adv. Mater.* **2004**, *16*, 1522–1525.
(8) Luo, W. F. *J. Alloys Compd.* **2004**, *381*, 284–287.
(9) Xiong, Z. T.; Hu, J. J.; Wu, G. T.; Chen, P.; Luo, W. F.; Gross, K. *J. Alloys Compd.* **2005**, *398*, 235–239.
(10) Leng, H. Y.; Ichikawa, T.; Hino, S.; Hanada, N.; Isobe, S.; Fujii, H. *J. Phys. Chem. B* **2004**, *108*, 8763–8765.
(11) Yang, J.; Sudik, A.; Wolverton, C. *J. Alloys Compd.* **2007**, *430*, 334–338.
(12) Liu, Y. F.; Zhong, K.; Gao, M. X.; Wang, J. H.; Pan, H. G.; Wang, Q. D. *Chem. Mater.* **2008**, *20*, 3521–3527.
(13) Xiong, Z. T.; Wu, G. T.; Hu, J. J.; Chen, P. *J. Power Sources* **2006**, *159*, 167–170.
(14) Lu, J.; Fang, Z. Z. *J. Phys. Chem. B* **2005**, *109*, 20830–20834.
(15) Xiong, Z. T.; Wu, G. T.; Hu, J. J.; Liu, Y. F.; Chen, P.; Luo, W. F.; Wang, J. *Adv. Funct. Mater.* **2007**, *17*, 1137–1142.
(16) Janot, R.; Eymery, J. B.; Tarascon, J. M. *J. Phys. Chem. C* **2007**, *111*, 2335–2340.
(17) Pinkerton, F. E.; Meisner, G. P.; Meyer, M. S.; Balogh, M. P.; Kundrat, M. D. *J. Phys. Chem. B* **2005**, *109*, 6–8.
(18) Pinkerton, F. E.; Meyer, M. S.; Meisner, G. P.; Balogh, M. P. *J. Phys. Chem. B* **2006**, *110*, 7967–7974.
(19) Chater, P. A.; David, W. I.; Johnson, S. R.; Edwards, P. P.; Anderson, P. A. *Chem. Commun.* **2006**, 2493–2441.
(20) Liu, Y. F.; Hu, J. J.; Wu, G. T.; Xiong, Z. T.; Chen, P. *J. Phys. Chem. C* **2007**, *111*, 19161–19164.
(21) Lu, J.; Fang, Z. Z.; Sohn, H. Y.; Bowman, R. C., Jr.; Hwang, S. J. *J. Phys. Chem. C* **2007**, *111*, 16686–16692.
(22) Chen, P.; Xiong, Z. T.; Luo, J. Z.; Lin, J. Y.; Tan, K. L. *J. Phys. Chem. B* **2003**, *107*, 10967–10970.
(23) Ichikawa, T.; Hanada, N.; Isobe, S.; Leng, H. Y.; Fujii, H. *J. Phys. Chem. B* **2004**, *108*, 7887–7892.
(24) David, W. I. F.; Jones, M. O.; Gregory, D. H.; Jewell, C. M.; Johnson, S. R.; Walton, A.; Edwards, P. P. *J. Am. Chem. Soc.* **2007**, *129*, 1594–1601.

10.1021/ja806565t CCC: $40.75

positively charged $H^{\delta+}$ in amide and the negatively charged $H^{\delta-}$ in hydride.[22] Almost simultaneously, Ichikawa et al. suggested the ammonia-mediated mechanism, in which amide decomposed to ammonia and imide/nitride and subsequently the ammonia just produced reacted with hydride to produce hydrogen.[23] Recently, a more detailed ion migration model was proposed by David et al. who suggested that the presence of Frenkel defect pairs in imide was the key in the dehydrogenation/hydrogenation process of metal−N−H system, and consequently the hydrogen absorption/desorption behavior depended strongly on the mobility of small ions both in amide and hydride.[24] By consideration of a solid-state reaction from the point of view of reaction kinetics, Chen et al. attributed the origin of kinetic barriers for dehydrogenation of the Li−Mg−N−H system to the interface reaction between amide and hydride to form a ternary imide in the preliminary stage and mass transport through the imide layer in the subsequent stage.[25] As a result, the reduction of particle size and the increase of the degree of mixing between reactants would effectively improve the rate of dehydrogenation reaction.

However, it is noteworthy that the previous investigations mainly took $Mg(NH_2)_2$ and LiH as the starting materials, and no positive measures have been taken to reduce the size of the subsequently reacting particles.[7−11] To fully dehydrogenate during the first dehydrogenation, the Li−Mg−N−H mixture was heated to a higher temperature (>220 °C), which inevitably made the particles grow in size and elevated the operating temperatures for subsequent hydrogenation and dehydrogenation. Here, for a better and more reactive particle size, a first attempt has been carried out to synthesize $Li_2MgN_2H_2$ by sintering a mixture of $Mg(NH_2)_2-2LiNH_2$, and subsequently the product was ball-milled for different periods to obtain particles of different sizes and to determine the effect of particle size on its hydrogenation/dehydrogenation kinetics. This work helped us to better understand the dehydrogenation mechanism of the Li−Mg−N−H system and shed some light on how to improve its dehydrogenation rate.

2. Experimental Section

2.1. Sample Preparation. Lithium amide ($LiNH_2$), a product of Alfa Aesar with 95% purity, was used as received. Magnesium amide ($Mg(NH_2)_2$) was synthesized in our own laboratory by reacting Mg power (99%, Sinopharm) with 7 atm ammonia at about 300 °C. The product was confirmed as $Mg(NH_2)_2$ by X-ray diffraction and infrared spectroscopy (see Supporting Information, Figure S1).

The mixture of $Mg(NH_2)_2$ and $LiNH_2$ at a molar ratio of 1:2 was first processed by ball-milling for 36 h on a planetary ball mill (QM-1SP4, Nanjing) rotating at 500 rpm and then subjected to a temperature-programmed heat treatment (Supporting Information, Figure S2). NH_3 was gradually evolved at temperatures above 150 °C and the first-step decomposition finished at 315 °C. The XRD pattern of the sample collected at 315 °C exhibits a $Li_2MgN_2H_2$ polymorph structure of both orthorhombic α-$Li_2MgN_2H_2$ structure and cubic β-$Li_2MgN_2H_2$ structure (Supporting Information, Figure S3). We believed that $Mg(NH_2)_2$ reacted with $LiNH_2$ to form a solid product of $Li_2MgN_2H_2$ with the generation of NH_3 at a temperature range of 150−315 °C:

$$Mg(NH_2)_2 + 2LiNH_2 \xrightarrow{150°C \text{ to } 315°C} Li_2MgN_2H_2 + 2NH_3 \quad (2)$$

In light of eq 2, $Li_2MgN_2H_2$ was produced by sintering the mixture of $Mg(NH_2)_2$ and $LiNH_2$ ball-milled for 36 h in this work. In a typical procedure, a premilled mixture of $Mg(NH_2)_2-2LiNH_2$ was put onto a stainless-steel-boat and loaded into a stainless steel tube, which was connected to a gas-circulating system and heated in a tube furnace. The powder mixture was heated with a ramp of 2 °C/min to 315 °C and held for 24 h under a constantly flowing pure nitrogen gas. Three $Li_2MgN_2H_2$ samples were prepared. Sample I was made by hand-milling the sintered sample in a mortar−pestle for 2 min. Samples II and III were prepared by ball-milling the sintered sample on a planetary ball mill (QM-1SP4, Nanjing), rotating at 500 rpm for 3 and 36 h, respectively. The ball-to-sample weight ratio was about 60:1. The handling of the reactants and products was all performed in a glovebox (MBRAUN) filled with a circulating pure argon to prevent air and moisture contamination (H_2O: <1 ppm, O_2: <1 ppm).

2.2. Hydrogen Absorption/Desorption Measurement. The hydrogen absorption/desorption performances and isothermal hydrogen desorption kinetics were determined quantitatively by a volumetric method with a homemade Sieverts-type apparatus. Typically, approximately 300 mg of sample was loaded in a glovebox into a homemade reactor which was then connected to a Sieverts-type apparatus. After outgassing under a primary vacuum (10^{-3} bar) at room temperature, the sample temperature was gradually raised to a preset temperature at 2 °C/min for hydrogen absorption/desorption. Simultaneously, a starting hydrogen pressure of 100 atm was applied for hydrogen absorption. Temperatures and pressures of the sample and gaseous reservoir were automonitored and recorded. The amounts of hydrogen for absorption/desortpion curves of the sample were calculated from the hydrogen pressures measured in the calibrated volume by using the ideal gas law. In the experiment for isothermal hydrogen desorption kinetics, the sample was quickly heated to and kept at the given temperature of 160 °C, and the gaseous pressure in the reactor was monitored as a function of time.

To calculate the apparent activation energy, temperature dependence of hydrogen desorption behavior of the hydrogenation sample was measured on a homemade temperature-programmed-desorption (TPD) system with an online gas chromatograph (GC) attached. The entire experiment procedure consisted of the following: the loading of about 50 mg of powder sample into a stainless steel tube in a glovebox, the connection of the tube to a gas-circulating system, and the heating of the tube in a tube furnace. A constant flow of pure Ar gas was sent through the sample while it was heated at a programmed rate (2−5 °C/min) from room temperature to 300 °C.

2.3. Structural Characterization. Structural identification was performed on a Rikagu D/Max-RA X-ray Diffractometer with Cu K_α radiation at 40 kV and 30 mA. X-ray diffraction (XRD) data were collected in the 2θ range 10° to 90° with a step increment of 0.05°. A homemade container was used to prevent powder samples from contacting air and moisture in the surrounding atmosphere.

N−H vibrations in all samples were identified by a Bruker Vector 22 Fourier infrared spectrometer (FTIR, Germany). The test sample was prepared by cold pressing a mixture of the powder samples and potassium bromide (KBr) powder at a weight ratio of 1:30 to form a pellet. Transmission mode was adopted, where the scan resolution was 4 cm^{-1} and 25 scans were made and accumulated.

The particle size of the sample milled for different periods was determined by a scanning electron microscope (Hitachi-4700, Japan). Samples were transferred quickly from a glovebox to the SEM facility with an air exposure time less than 30 s. Elemental nitrogen can still be detected by an energy dispersive X-ray spectrometer (EDS).

3. Results and Discussion

3.1. Hydrogenation Behavior of $Li_2MgN_2H_2$ Samples after Different Milling Treatments. First, the hydrogenation behaviors of the $Li_2MgN_2H_2$ samples after being hand-milled and ball-milled for 3 and 36 h with the temperature increased to 210 °C were investigated, and the hydrogen absorption curves are shown

(25) Chen, P.; Xiong, Z. T.; Yang, L. F.; Wu, G. T.; Luo, W. F. *J. Phys. Chem. B* **2006**, *110*, 14221–14225.

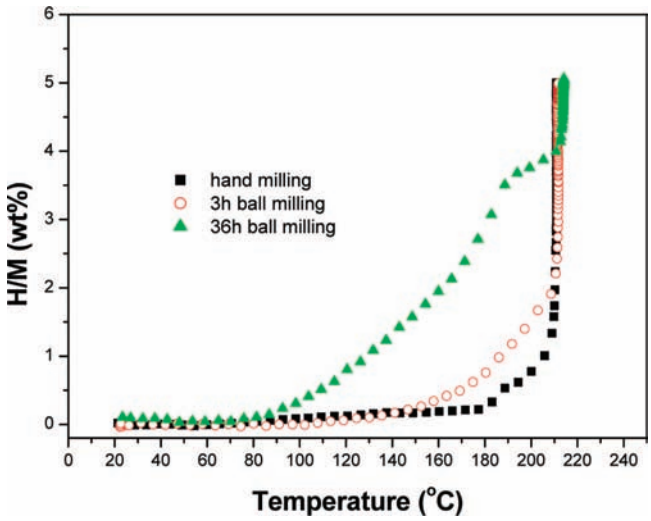

Figure 1. Hydrogenation curves of $Li_2MgN_2H_2$ samples subjected to different treatments with H/M versus temperature.

in Figure 1. All samples absorb about 5 wt% of hydrogen at 210 °C under 100 atm of hydrogen pressure, very close to the theoretical capacity of 5.5 wt%. It is interesting to note that the onset temperature for hydrogen absorption is significantly lowered after the sample was ball-milled. The onset of hydrogen absorption for the hand-milled sample is 180 °C, whereas the sample ball-milled for 36 h starts to absorb hydrogen at only 80 °C, and it absorbs about 3 wt% of hydrogen at 180 °C. Therefore the ball-milling treatment appears to have the ability to dramatically reduce kinetic barriers for the hydrogenation reaction of $Li_2MgN_2H_2$ due probably to the reduction in the particle size and defects created by fracturing and cold welding of the elemental constituent particles during ball-milling.[26]

3.2. Structure and Particle Size of $Li_2MgN_2H_2$ Samples after Different Milling Treatments. With the aim of elucidating the significant reduction in the hydrogen absorption temperature, structure examinations have been performed on the $Li_2MgN_2H_2$ samples before and after ball-milling by means of XRD and FTIR. Figure 2a shows XRD patterns of the $Li_2MgN_2H_2$ samples after being hand-milled and ball-milled for 3 and 36 h. Apparently, the hand-milled sample exhibits a $Li_2MgN_2H_2$ polymorph structure, and all diffraction peaks can be attributed to the orthorhombic α-$Li_2MgN_2H_2$ (space group *Iba*2, a = 9.7837 Å, b = 4.9893 Å, c = 5.1984 Å) and the cubic β-$Li_2MgN_2H_2$ (space group $P\bar{4}_3m$, a = 5.0268 Å) as reported by Rijssenbeek et al. and Hu et al.[27,28] All diffraction peaks are sharp, indicating a regular crystalline $Li_2MgN_2H_2$ powder. After 3 h of ball-milling, it is interesting to note that the typical diffraction peaks of the orthorhombic α-$Li_2MgN_2H_2$ disappear and, only five peaks at 17.3°, 30.7°, 42.7°, 51.2°, and 61.1° corresponding to the cubic β-$Li_2MgN_2H_2$ phase are discernible. This fact signifies a polymorphic transformation occurs from the orthorhombic α-$Li_2MgN_2H_2$ phase to the cubic β-$Li_2MgN_2H_2$ phase probably because the orthorhombic phase has lower symmetry and hence is less stable than the cubic phase. According to Rijssenbeek's report,[27] the orthorhombic α-$Li_2MgN_2H_2$ phase transfers gradually to the cubic β-$Li_2MgN_2H_2$ phase with higher symmetry at 350 °C. In general, a high pressure in the order of GPa is generated in the solid particle by colliding balls during energetic ball-milling,[26] which possibly provides the driving force for the polymorphic transformation of $Li_2MgN_2H_2$ from the orthorhombic α-phase to the cubic β-phase. In addition, the diffraction peaks are obviously broadened and their intensities are lowered, signifying the decrease in particle size and crystallite size and an increase in defects. When the ball-milling is prolonged to 36 h, the diffraction patterns remain almost unchanged except that the peaks are further broadened and their intensities are further depressed. The crystallite sizes based on the strongest peak direction for the $Li_2MgN_2H_2$ samples after being hand-milled and ball-milled for 3 and 36 h respectively are calculated according to Scherrer equation to be ca. 41, 29, and 25 nm, proving quantitatively the decrease in the crystallite size due to ball-milling. It is also worth noting that the crystallite size of the sample reduces dramatically from 41 to 29 nm only in 3 h of ball-milling, which correlates well with the difference of the unit cell parameters between the orthorhombic α-phase and the cubic β-phase,[27] further proving the occurrence of the phase transformation of $Li_2MgN_2H_2$ from the orthorhombic α-phase to the cubic β-phase during ball-milling.

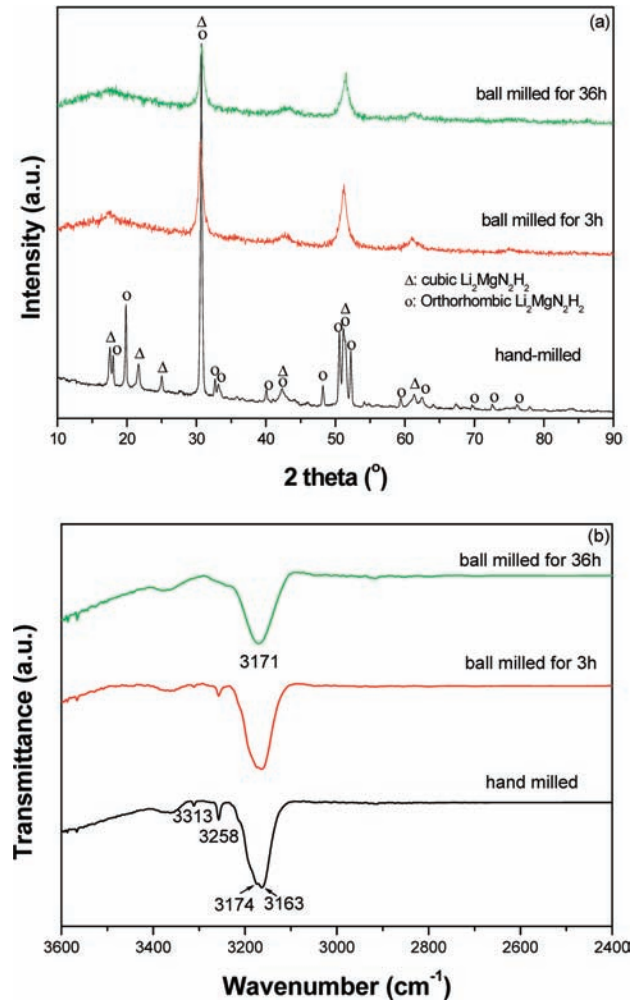

Figure 2. XRD patterns (a) and FTIR spectra (b) of $Li_2MgN_2H_2$ samples with different treatments.

Infrared spectroscopy is also a powerful technique for the characterization of amides and imides, as the vibration bands

(26) Bérubé, V.; Radtke, G.; Dresselhaus, M.; Chen, G. *Int. J. Energy Res.* **2007**, *31*, 637–663.
(27) Rijssenbeek, J.; Gao, Y.; Hanson, J.; Huang, Q. Z.; Jones, C.; Toby, B. *J. Alloys Compd.* **2008**, *454*, 233–244.
(28) Hu, J. J.; Liu, Y. F.; Wu, G. T.; Xiong, Z. T.; Chen, P. *J. Phys. Chem. C* **2007**, *111*, 18439–18443.

associated to their covalent N−H bonds are in quite different positions. Figure 2b shows the FTIR spectra of the $Li_2MgN_2H_2$ samples after being hand-milled and ball-milled for 3 and 36 h. For the hand-milled sample, the absorbance in the N−H vibration range of imide resembles a whole broad peak centered at 3171 cm^{-1} at first sight. However, a closer examination shows that it is composed of two peaks at 3174 and 3163 cm^{-1}. In the meantime two weak absorbances at 3313 and 3258 cm^{-1} can also be observed, which may be originated from the unreacted $LiNH_2$. Very weak intensity of the absorbances at 3313 and 3258 cm^{-1} indicates the concentration of $LiNH_2$ in the sintered product is too low to be detected by means of XRD in Figure 2a. After 3 h of ball-milling, two peaks at 3174 and 3163 cm^{-1} incorporate gradually into a single one. This fact is more structural evidence for the occurrence of the phase transformation of $Li_2MgN_2H_2$ from the orthorhombic α-phase to the cubic β-phase. When the length of ball-milling goes up to 36 h, only a symmetric single absorbance at 3171 cm^{-1} is discernible, which agrees well with our previous result studied on the cubic $Li_2MgN_2H_2$ phase.[29]

For a quantitative comparison of the particle size, SEM was employed to examine the morphologies of the powder samples after being hand-milled and after being ball-milled for 3 and 36 h, respectively. SEM micrographs are presented in Figure 3. The particles of the hand-milled sample are very irregular in shape and size with little agglomeration of particles. The sizes of most part of particles are larger than 800 nm (Figure 3a). After 3 h of ball-milling, particles become near-spherical and more uniform in size as shown in Figure 3b. The particle sizes are then reduced to 300−400 nm. As the ball-milling is prolonged to 36 h, the size of particles of the sample is reduced to 100−200 nm (Figure 3c). It is generally accepted that, for most chemisorption-based hydrogen storage materials, the smaller the particles, the lower the H_2 absorption/desorption temperature because of the larger external surface area and the lower surface activation energy.[30,31] The hydrogenation curves of $Li_2MgN_2H_2$ samples with different milling treatments as shown in Figure 1 have experimentally supported our inference. In-depth investigation on the dehydrogenation behavior of $Li_2MgN_2H_2$ samples hydrogenated at 210 °C is reported in the following section.

3.3. Dehydrogenation/Rehydrogenation Behavior of $Li_2MgN_2H_2$ Samples Hydrogenated at 210 °C. The dehydrogenation behaviors of $Li_2MgN_2H_2$ samples with different milling treatments after being hydrogenated at 210 °C were then examined. Figure 4a shows the hydrogen desorption curves of three hydrogenated samples. Three samples in this test exhibit very similar dehydrogenation behavior, namely the H/M versus temperature curve and the same total hydrogen desorption amount of 5 wt% at 260 °C, equivalent to the amount of hydrogen absorbed, indicating a complete reversible hydrogen storage process of $Li_2MgN_2H_2$. In the meantime it should be noted that the hydrogen desorption kinetics is slightly improved after being ball-milled. The onset temperature for hydrogen desorption from the hydrogenated hand-milled sample is about 165 °C, whereas the hydrogenated ball-milled sample for 36 h starts to desorb hydrogen at about 150 °C. In the temperature range of 150−210 °C, the operating temperature for hydrogen desorption of the sample ball-milled for 36 h is slightly lower than that for the hand-milled sample. The three hydrogen desorption curves meet at 212 °C.

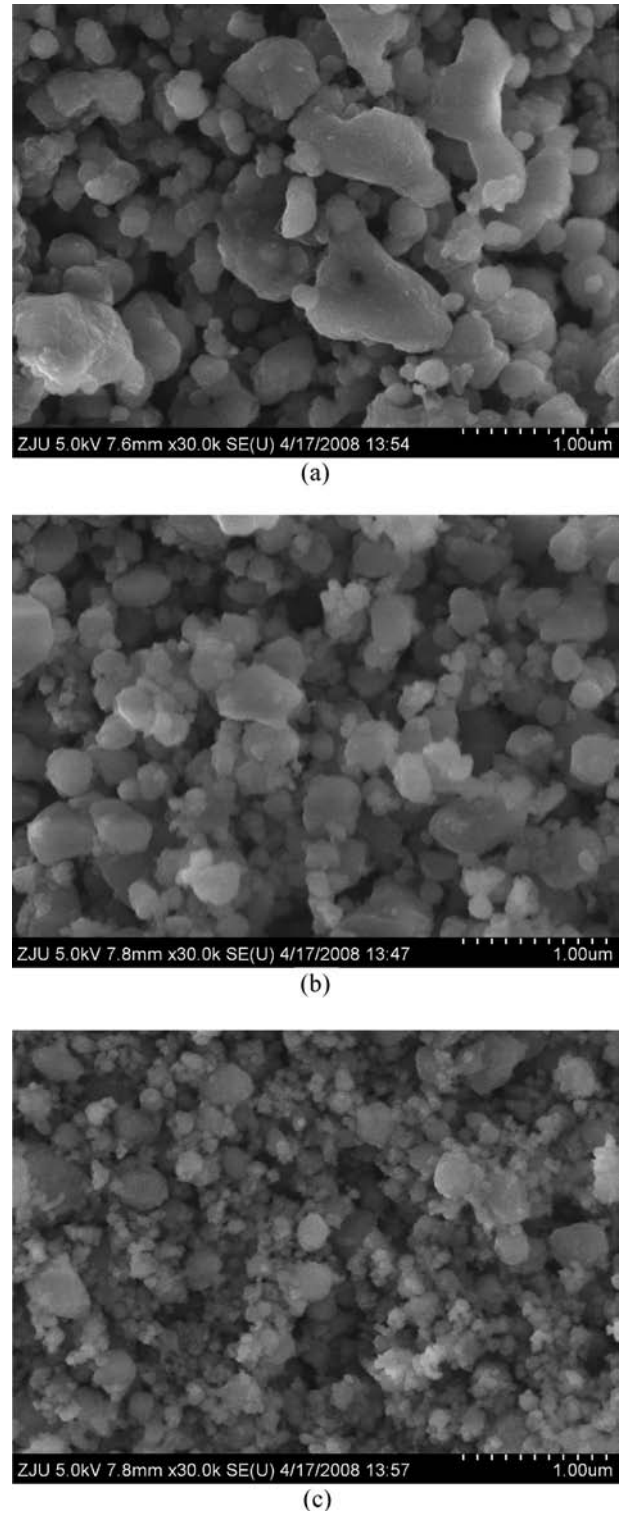

Figure 3. SEM micrographs of $Li_2MgN_2H_2$ samples after being hand-milled (a) and ball-milled for 3 h (b) and for 36 h (c).

After dehydrogenation at 260 °C, rehydrogenation was carried out on three samples under the same conditions as the first hydrogenation. The results are shown in Figure 4b. Unlike the first hydrogenation, three samples show very similar rehydro-

(29) Liu, Y. F.; Hu, J. J.; Xiong, Z. T.; Wu, G. T.; Chen, P. *J. Mater. Res.* **2007**, *22*, 1399–1345.
(30) Baldé, C. P.; Hereijgers, B. P. C.; Bitter, J. H.; de Jong, K. P. *J. Am. Chem. Soc.* **2008**, *130*, 6761–6765.
(31) Li, W. Y.; Li, C. S.; Ma, H.; Chen, J. *J. Am. Chem. Soc.* **2007**, *129*, 6710–6711.

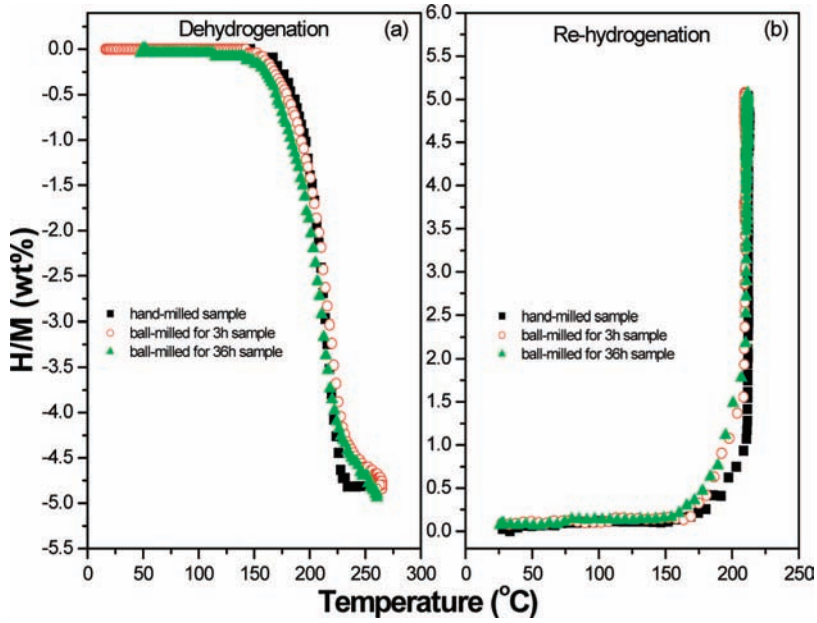

Figure 4. Dehydrogenation (a) and rehydrogenation (b) curves of $Li_2MgN_2H_2$ samples hydrogenated at 210 °C.

genation behavior, and no remarkable improvement in hydrogenation performance is observed for the ball-milled samples. It is worth highlighting to point out that ball-milling has made a significant improvement on the first hydrogen absorption but has only little influence on the subsequent dehydrogenation/rehydrogenation as shown in Figure 4.

For solid-state reaction of powder samples, since the particle size of powder sample is one of the most important influence factors for the reaction kinetics, we believe that the growth and/or agglomeration of the sample particles during hydrogenation at the relative higher operating temperature of 210 °C to be the cause for the deterioration of the subsequent dehydrogenation/rehydrogenation behavior. To justify our judgment, the samples hand-milled and ball-milled for 36 h were taken as examples, and the morphologies of these particles after hydrogenation at 210 °C were observed with SEM and are shown in Figure 5. After hydrogenation at 210 °C, the initially separated particles are aggregated and the particle size is augmented, especially for the sample ball-milled for 36 h. The particle size of the sample ball-milled for 36 h is increased from the initial 100−200 nm to 700−800 nm, only slightly smaller than that of the hydrogenated hand-milled sample (~1 μm). We believe the final and rather close particle size is responsible for the quite similar dehydrogenation behavior. The comparatively high operating temperature used for hydrogen absorption gave rise to the very adverse effect on the subsequent hydrogen desorption.

3.4. Hydrogenation/Dehydrogenation Behavior of $Li_2MgN_2H_2$ Samples at Different Temperatures. To further investigate the effect of the particle size of the hydrogenated $Li_2MgN_2H_2$ samples on the dehydrogenation behavior, samples after being hand-milled (sample I) and ball-milled for 3 h (sample II) and for 36 h (sample III) were first hydrogenated at 240, 210, and 160 °C, respectively, and subsequently dehydrogenated experimentally. Figure 6 exhibits the hydrogen absorption/desorption curves of these three samples. Their hydrogen absorption all amounts to 5 wt% at 240, 210, and 160 °C, respectively. Specifically, Sample III, the $Li_2MgN_2H_2$ sample ball-milled for 36 h, can be completely hydrogenated even at the low operating temperature of 160 °C if enough holding time is given. After being hydrogenated at different temperatures, the dehydrogenation behavior of sample II is very close to that of sample I, whereas sample III is quite discrepant displaying a big decrease

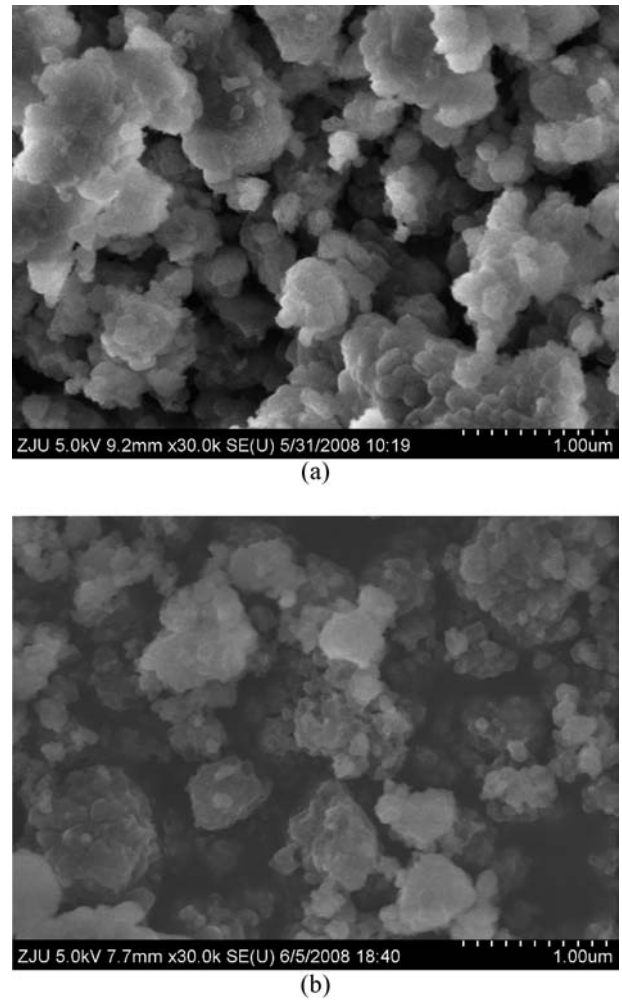

Figure 5. SEM micrographs of $Li_2MgN_2H_2$ samples after being hydrogenated at 210 °C. (a) Hand-milled sample; (b) sample ball-milled for 36 h.

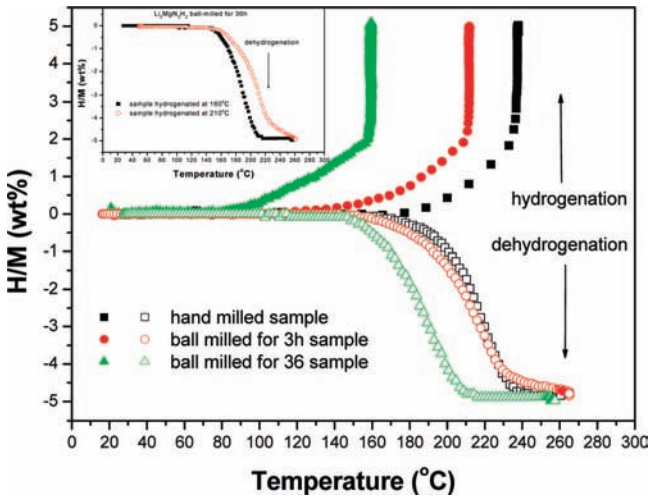

Figure 6. Hydrogenation/dehydrogenation curves of $Li_2MgN_2H_2$ samples with different milling treatments.

in the dehydrogenation temperature. More inspiringly, the end temperature of hydrogen desorption for sample III lowers dramatically from 260 to 215 °C relative to that for the hand-milled sample. For the dehydrogenation experiments of the hydrogenated sample III at 160 and 210 °C, similar improvement in dehydrogenation kinetic is observed with their onset temperatures for hydrogen desorption almost same (i.e., 150 °C) but with a 45 °C difference in the end temperature as shown in the insert of Figure 6.

The fact of the noticeable discrepancy in the hydrogen desorption behavior arises our investigation interest on the morphologies of the samples hydrogenated at different temperatures. Figure 7 presents the SEM micrographs of the hydrogenated samples I, II, and III at 240, 210, and 160 °C, respectively. Apparently, most of the particles of sample I grow to above 1 μm by agglomerating with small particles after being hydrogenated at 240 °C. Sample II also exhibits a distinct increase in particle size from 300−400 nm to 700−800 nm after being hydrogenated at 210 °C. Nevertheless, the resultant particles of sample III hydrogenated at 160 °C have a size range of 300−400 nm, at only about 1/3 of the particle size of the hydrogenated sample I although the conglomeration of small particles can be obviously observed as well in Figure 7c. As a result, we believe that the final particle size is strongly responsible for the lower end temperature of hydrogen desorption of sample III, and that the decrease in the operating temperature for hydrogenation/dehydrogenation effectively restrains the increase in the particle sizes of the powder samples, consequently enhancing the hydrogen absorption/desorption kinetics during hydrogenation/dehydrogenation cycling.

3.5. Isothermal Desorption Kinetics of Hydrogenated $Li_2MgN_2H_2$. Hydrogen desorption behaviors of $Li_2MgN_2H_2$ samples with different treatments in the temperature range of 20−270 °C have been roughly examined in the last section and are shown in Figure 6. The results indicate that the nonisothermal kinetics of hydrogen desorption is dramatically improved by reducing the particle size of the reactants. Previous investigations on the hydrogen desorption kinetics of the Li−Mg−N−H system attributed the origin of its kinetic barriers to the interface reaction between amide and hydride to form ternary imide in the preliminary stage and mass transport through the imide layer in the subsequent stage.[25] However, the rate-controlling step for hydrogen desorption has not explicitly identified experimentally yet. Therefore, it is still worthy to elaborate the mechanism on reaction kinetics for the hydrogen desorption of the Li−Mg−N−H system. In the following text, the examinations on isothermal kinetics were carried out on the hydrogenated hand-milled and ball-milled samples to determine the rate-controlling step for hydrogen desorption.

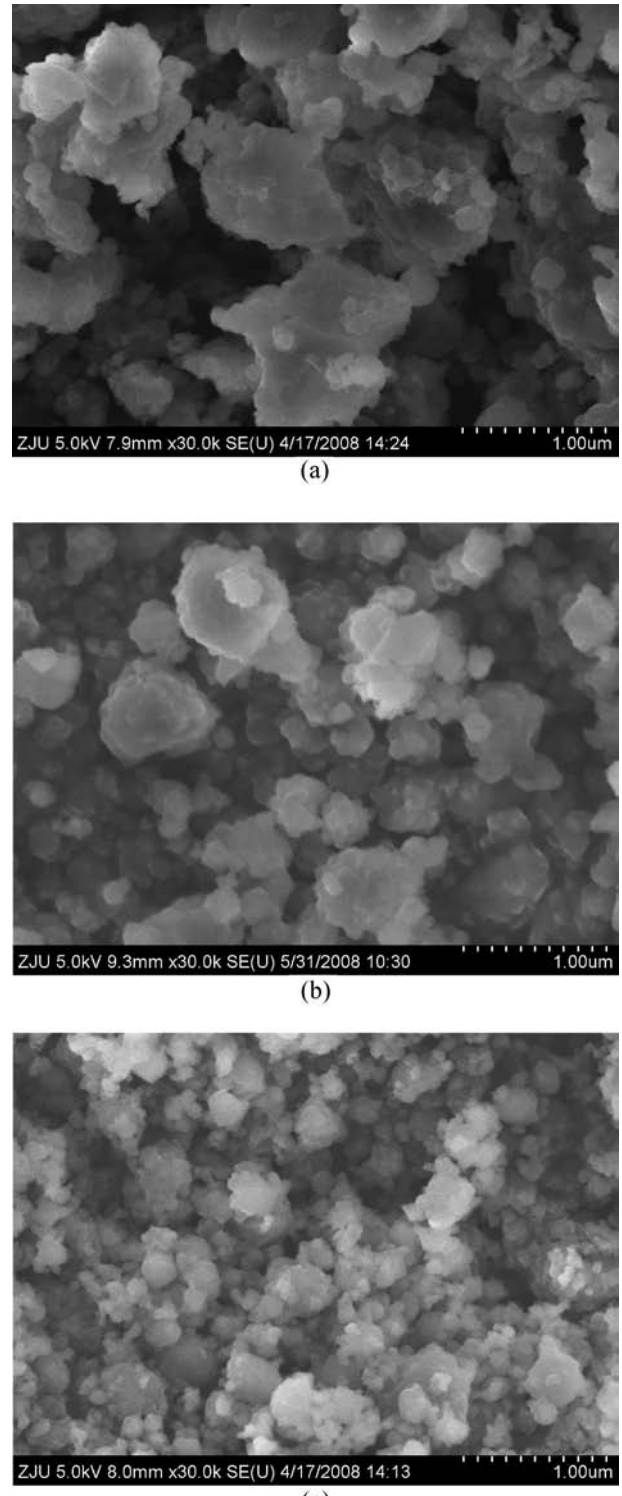

Figure 7. SEM micrographs of $Li_2MgN_2H_2$ samples after being hydrogenated at different temperatures. (a) Hydrogenated hand-milled sample at 240 °C; (b) hydrogenated ball-milled for 3 h sample at 210 °C; (c) hydrogenated ball-milled for 36 h sample at 160 °C.

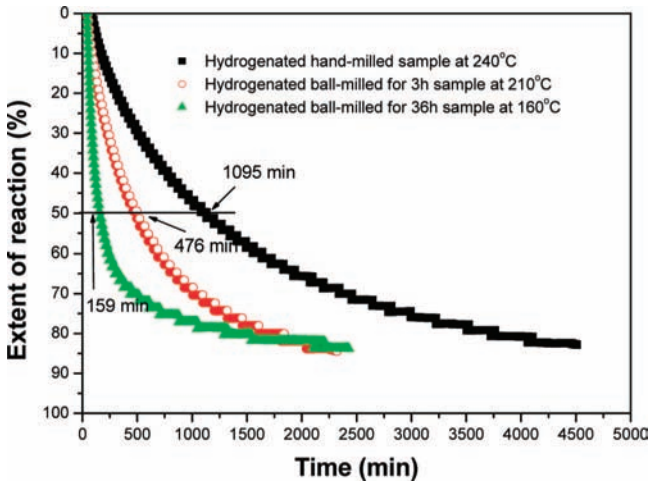

Figure 8. Isothermal dehydrogenation curves (at 160 °C) of hydrogenated $Li_2MgN_2H_2$ samples.

The samples after being hand-milled (sample I) and ball-milled for 3 h (sample II) and for 36 h (sample III) were first completely hydrogenated at 240, 210, and 160 °C, respectively, and then desorbed at 160 °C. Figure 8 shows the time dependence of the extent of the reaction of hydrogen desorption of the three samples at 160 °C. The extent of reaction was calculated from the amount of hydrogen desorbed from the sample. As shown in Figure 8, more than 80% of hydrogen storage capacity can be desorbed from three hydrogenation samples at 160 °C with quite different desorption rates. The hydrogen desorption curve of the hydrogenated sample I is parabolic, while the curve of the hydrogenated sample III is composed of a linear region and a parabolic region, signifying that the hydrogen desorption kinetics of the hydrogenated sample III is much higher than that of the hydrogenated sample I. It takes only 159 min to desorb 50% of hydrogen from the sample III hydrogenated at 160 °C, but 1095 min are required to desorb the same amount of hydrogen for the sample I hydrogenated at 240 °C.

In general, the reaction rate of a thermally activated solid-state reaction can be expressed by the following equation:[32]

$$\text{rate} = \frac{d\alpha}{dt} = k(T)f(\alpha) \quad (3)$$

in which α is the extent of the reaction ranging from 0 when the reaction starts to 1 when it completes, t is the time, T is the absolute temperature, $k(T)$ is a temperature-dependent reaction rate constant, and $f(\alpha)$ is a term for the reaction rate which is dependent on the reaction mechanism. Several solid-state reaction mechanism models have been proposed including the nucleation, the geometrical contraction, the diffusion, and the reaction order models based on the different geometry of the particles and the different driving forces. Many different rate expressions have also been derived from these mechanisms.[33−39] Several most commonly used mechanisms are listed in Table S1, Supporting Information.

To identify the solid-state reaction mechanism, it is necessary first to select a proper model which involves all essential chemical steps. A practical approach for the rapid selection of an appropriate rate equation for the kinetics of an isothermal solid-state reaction has been made by Sharp et al.[40] They recast the rate equations listed in Table S1 in the following form:

$$f(\alpha) = A(t/t_{0.5}) \quad (4)$$

wherein $t_{0.5}$ is the time when $\alpha = 0.5$ and A is a constant depending on kinetic model. Taking the well-known contracting expression (R2 model listed in Table S1) as an example,

$$R_2(\alpha) = 1 - (1-\alpha)^{1/2} = kt \quad (5)$$

When $\alpha = 0.5$,

$$R_2(0.5) = 0.293 = kt_{0.5} \quad (6)$$

Thus,

$$k = 0.293/t_{0.5} \quad (7)$$

Therefore, eq 5 can be rewritten as:

$$R_2(\alpha) = 0.293(t/t_{0.5}) \quad (8)$$

By plotting the experiment data $f(\alpha)$ against $t/t_{0.5}$, the rate constant evaluated from the linear slope of the plot can be found. On comparing the slope thus with the theoretical slopes, the reaction mechanism can be determined. The theoretical values of α and $t/t_{0.5}$ for some commonly used solid-state reaction equation have been calculated by Sharp et al. (Table S2, Supporting Information). However, it is generally preferable to use methods of analysis which produce a linear plot rather than the method of comparing with theoretical curves. On the basis of Sharp's work, Jones et al. developed a more facilely exact method to identify the reaction mechanism by plotting the relationship of the experimental data $(t/t_{0.5})_{exp}$ versus the theoretical data $(t/t_{0.5})_{theo}$ of different rate equations to produce a linear plot.[41] The value of the linear slop of an acceptable model should be very close to 1.

In the present study, Jones's method was adopted and the experimental value $(t/t_{0.5})_{exp}$ was plotted against $(t/t_{0.5})_{theo}$ of nine different kinetic mechanisms listed in Table S1, respectively, for the determination of the dehydrogenation mechanism of the Li−Mg−N−H system. Figure 9 shows the relationship of $(t/t_{0.5})_{exp}$ versus $(t/t_{0.5})_{theo}$ of the three samples for nine different kinetic mechanisms, and the linear slopes found are listed above the graphs in the figure. For samples I and II, the $(t/t_{0.5})_{exp}$ value plotted against the $(t/t_{0.5})_{theo}$ value of the D4 model exhibits a good linear relationship with slopes close to 1, whereas for sample III, it should be the D3 model. In physical chemistry, the D3 model is known as Jander equation, and the D4 model as Ginstling−Braunshteinn equation. Both of them represent a 3-D diffusion reaction mechanism. This finding indicates that the hydrogen desorption reaction of the hydrogenated $Li_2MgN_2H_2$ sample correlates closely to the 3-D diffusion mechanism. Recently, a detailed ion migration model has been proposed for the hydrogenation/dehydrogenation reaction of the

(32) Davydov, E. Y. *Kinetic Peculiarities of Solid Phase Reactions*; John Wiley & Sons, Ltd.: New York, 1998.
(33) Ginstling, A. M.; Brounshteĭn, *J. Appl. Chem USSR (Engl. Transl.)* **1950**, *23*, 1327–1338.
(34) Valensi, G. *Compt. Rend.* **1936**, *202*, 309–312.
(35) Carter, R. E. *J. Chem. Phys.* **1961**, *34*, 2010–2015.
(36) Holt, J. B.; Culter, I. B.; Wadsworth, M. E. *J. Am. Ceram. Soc.* **1962**, *45*, 133–136.
(37) Jander, W. *Z. Anorg. Allgem. Chem.* **1927**, *163*, 1–30.
(38) Avrami, M. *J. Chem. Phys.* **1939**, *7*, 1103–1112.
(39) Erofe'ev, B. V. *Compt. Rend. Acad. Sci. URSS* **1946**, *52*, 511–514.
(40) Sharp, J. H.; Brindley, G. W.; Achar, B. N. N. *J. Am. Ceram. Soc.* **1966**, *49*, 379–382.
(41) Jones, L. F.; Dollimore, D.; Nicklim, T. *Therm. Acta* **1975**, *13*, 240–245.

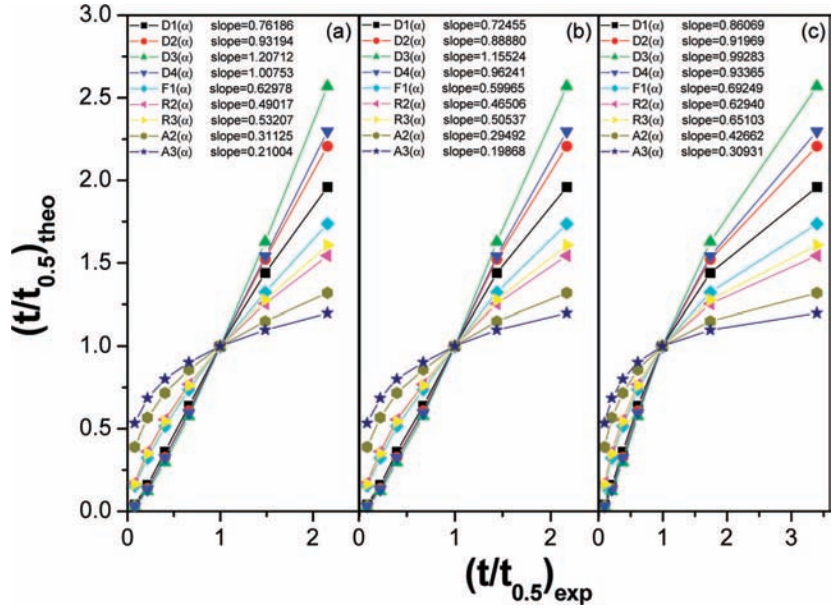

Figure 9. $(t/t_{0.5})_{theo}$ vs $(t/t_{0.5})_{exp}$ of hydrogenated $Li_2MgN_2H_2$ samples for various solid-state reaction equations. (a) Hand-milled sample; (b) sample ball-milled for 3 h; (c) sample ball-milled for 36 h.

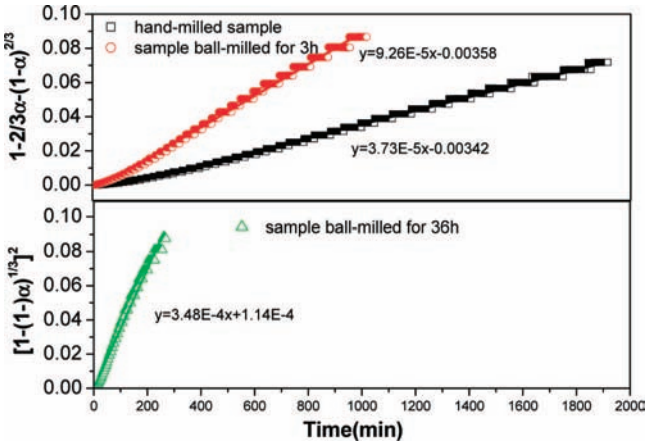

Figure 10. Time dependence of $f(\alpha)$ for the dehydrogenation of the hydrogenated hand-milled and ball-milled samples.

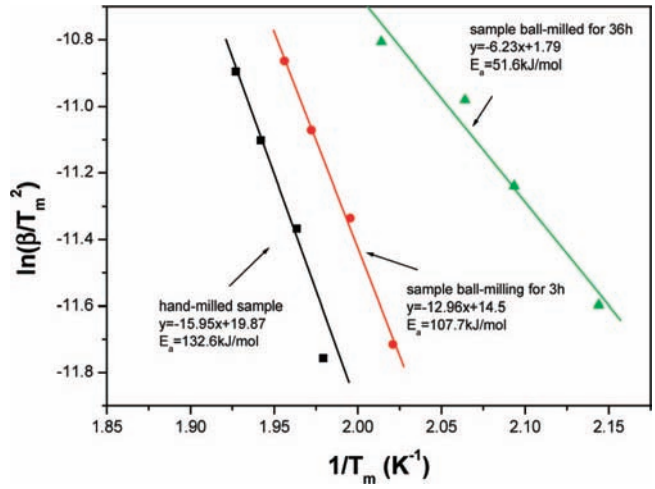

Figure 11. Kissinger plots of hydrogenated hand-milled and ball-milled $Li_2MgN_2H_2$ samples.

amide−hydride system from the structural point of view.[24,42] David et al. proposed that the hydrogenation/dehydrogenation process of the Li−N−H system is driven by Li^+ and H^+ mobility within the lithium imide on the basis of the observation of the nonstoichiometric imide.[24] In this model, the principal step is the movement of Li^+ in $LiNH_2$ to create a short-lived Frenkel defect pair, charged interstitial $[Li_iLiNH_2]^+$, and a lithium vacancy $[_{Li}\square NH_2]^-$. Taking into account the similar size of Mg^{2+} and Li^+, Wu et al. believed further that the hydrogen storage of $Li_2MgN_2H_2$ should also depend strongly on the migration of small mobile ions such as Li^+, H^+, and H^-.[42] These mechanistic understandings convince us that the rate-controlling step for the dehydrogenation of the Li−Mg−N−H system should be in fact the diffusion of the mobile small ions in both the amide and hydride.

On the basis of above investigations, the isothermal hydrogen desorption kinetics proceeded according to Ginstling−Braunshteinn equation for samples I and II and according to Jander equation for sample III. The results are shown in Figure 10. In the range of $\alpha = 0.1-0.7$, the time dependence of $f(\alpha)$ exhibits good linear relationship for the three samples, implying their reaction behaviors can be reasonably interpreted by the Ginstling−Braunshteinn equation and the Jander equation, respectively. Since the particles of the hydrogenated sample III at 160 °C are small and uniform as shown in Figure 7, their hydrogen desorption behavior practically satisfies the assumption of Jander equation. For the hydrogenated sample I at 240 °C, however, their particles are large and uneven, and their isothermal hydrogen desorption process can be well described by the Ginstling−Braunshteinn equation. The rate constant calculated by fitting the linear slope are 3.73×10^{-5}, 9.26×10^{-5}, and 3.48×10^{-4} s^{-1} for dehydrogenation reactions of the hydrogenated samples I, II, and III, respectively, indicating quantitatively the improvement of their hydrogen desorption kinetics.

For realizing more deeply the enhancement of the rate constant, the activation energies (E_a) of three samples were further evaluated with Kissinger method[43] and the results are shown in Figure 11. The E_a for the hydrogenated sample I was

(42) Wu, H. *J. Am. Chem. Soc.* **2008**, *130*, 6515–6522.

calculated to be 132.6 kJ/mol, and it is 107.7 kJ/mol for the hydrogenated sample II. Excitingly, the E_a calculated is only 51.6 kJ/mol for the hydrogenated sample III, with a dramatic 61% decrease in E_a relative to sample I. The fact indicates that the reduction in the particle size is very effective for lowering the energy barriers associated with ionic diffusion. In other words, the diffusion kinetics of small ions in the samples is distinctly improved by the decrease of particle size and the increase of the defect induced by energetic ball-milling. As a consequence, an improvement of the hydrogenation/dehydrogenation kinetics can be achieved in fact.

4. Conclusion

In this paper, $Li_2MgN_2H_2$ was first synthesized by sintering the premilled $Mg(NH_2)_2-2LiNH_2$ mixture at 315 °C, and the effect of particle size made by energetic ball-milling on its hydrogenation/dehydrogenation kinetics was systematically investigated. XRD and IR examinations showed that a polymorphic transformation was induced from the orthorhombic α-$Li_2MgN_2H_2$ phase to the cubic β-$Li_2MgN_2H_2$ phase during ball-milling. SEM observation found that the particle size of the sample is dramatically reduced from >800 nm to 100−200 nm after 36 h of ball-milling. Investigations on hydrogen absorption/desorption performances indicated that the onset of hydrogen absorption for the sample ball-milled for 36 h was dramatically lowered to 80 °C, and its dehydrogenation kinetics was significantly improved as well after hydrogenation at a much lower temperature (160 °C). The rate-controlling step of hydrogen desorption reaction was identified to be diffusion of small ions in the sample using a linear plot method. The isothermal hydrogen desorption process of the hand-milled and ball-milled for 3 h samples can be well described by Ginstling−Braunshteinn equation, and the sample ball-milled for 36 h fits Jander equation well. The rate constant evaluated by fitting the linear slope are enhanced from 3.73×10^{-5} s^{-1} for hand-milled sample to 3.48×10^{-4} s^{-1} for the sample ball-milled for 36 h. The activation energy calculated by Kissinger method only is 51.6 kJ/mol for the sample ball-milled for 36 h hydrogenated at 160 °C, with a dramatic 61% decrease relative to the hand-milled sample hydrogenated at 240 °C.

Acknowledgment. The authors would like to acknowledge the financial supports from National Natural Foundation of China (Grant 50631020 and 50701040), from National High-Technology Research and Development Plan (863 Program, Grant 2006AA05Z127), from Qianjiang Talent Project of Zhejiang Province (Grant QJD0702005), and from the Scientific Research Foundation of the State Education Ministry for Returned Overseas Chinese Scholars.

Supporting Information Available: XRD and FTIR of $Mg(NH_2)_2$; thermal decomposition of $Mg(NH_2)_2-2LiNH_2$; XRD of sintered $Li_2MgN_2H_2$; solid-sate rate expressions; theoretical values of α and $t/t_{0.5}$ for various kinetic models. This material is available free of charge via the Internet at http://pubs.acs.org.

JA806565T

(43) Kissinger, H. E. *Anal. Chem.* **1957**, *29*, 1702–1706.